Pharmaceutical Sciences and Drug Design
ISSN: 3062-4428
2026, Volume 6, Issue 1, Page No: 201-219

Available online at: www.galaxypub.co/page/journals

Galaxy Publication

Galaxy Publication

Caffeine-Loaded Mesoporous Silica Nanoparticles as a Dual-Pathway Therapeutic Strategy in Benzene-Induced Acute Myeloid Leukemia

James Walker[1]*, Olivia Harris[1]

[1]Department of Pharmaceutical Sciences and Therapeutic Design, Faculty of Medicine and Health Sciences, University of Edinburgh, Edinburgh, United Kingdom.

***E-mail** ✉ james.walker@gmail.com

Received: 14 February 2026; **Revised:** 11 April 2026; **Accepted:** 14 April 2026

ABSTRACT

Breakthroughs in nanoscience have sparked a radical rethinking of how therapeutically valuable natural compounds are applied in medicine. This investigation seeks to engineer a nanoformulated natural product for potent cancer therapy. Toward this end, mesoporous silica nanoparticles (MSNPs) were prepared, thoroughly characterized, and then loaded with caffeine to construct a site-specific drug carrier, referred to as caffeine-coated nanoparticles (CcNPs). Computational docking simulations were performed to probe the binding affinity of the CcNPs to a panel of apoptotic protein targets, followed by in vitro and in vivo biological evaluations using relevant animal models. Free caffeine, the nano-encapsulated caffeine formulation, and doxorubicin were each introduced intravenously into a benzene-initiated AML rodent model. Anti-leukemic activity was assessed by blood profiling, enzymatic biomarker quantification, and RT-PCR-based analysis of molecular shifts in leukemic markers. The docking data indicated potent intermolecular binding between CcNPs and apoptotic regulators. In vitro findings revealed antioxidant effects of clear statistical significance, while in vivo results indicated a return to baseline expression levels of the leukemic markers STMN1 and S1009A, along with the re-establishment of normal blood cell morphology and hematological parameters in animals receiving the nano-therapy. A parallel marked recovery in hepatic and kidney function markers was also recorded. In addition to these effects, the nano-formulation restored aberrantly high GAPDH and mTOR expression driven by benzene to physiological levels. The treatment further diminished pro-survival signaling through the NF-kappa B cascade and lifted P53 expression. With respect to the TRAIL axis, it enhanced the expression of the death-promoting factors TRAIL and DR5 while suppressing the anti-apoptotic mediator cFLIP. The body of evidence indicates that caffeine-laden MSNPs, designated CcNP/nanomedicine, can suppress the expansion of transformed cells and activate the cell-death-promoting TRAIL pathway to counteract benzene-driven leukemia. These observations establish our nano-therapeutic as a remarkably promising interventional option for AML.

Keywords: Acute myeloid leukemia, Docking, Caffeine, MSNPs, Nanomedicine, Doxorubicin

How to Cite This Article: Walker J, Harris O. Caffeine-Loaded Mesoporous Silica Nanoparticles as a Dual-Pathway Therapeutic Strategy in Benzene-Induced Acute Myeloid Leukemia. Pharm Sci Drug Des. 2026;6(1):201-19. https://doi.org/10.51847/Y41IB4uFAf

Introduction

The designation “cancer” covers a collection of illnesses marked by unrestrained cellular multiplication and encroachment into neighboring tissue [1]. In oncology, leukemia is a disorder in which hematopoietic precursors residing in the bone marrow undergo neoplastic transformation, leading to an overabundance of leukocytes, or white blood cells [2]. This state produces a surge of immature white cells in peripheral circulation alongside a shortfall in the generation of functional erythrocytes, lymphocytes, and thrombocytes. From a clinical standpoint, the detection of blast forms accounting for no less than 30% of cellular composition upon hematological review substantiates an acute myeloid leukemia (AML) diagnosis [3]. In AML treatment, established therapeutic modalities include chemotherapy, radiotherapy, surgical intervention, endocrine-based treatments, and immune-directed strategies.

Beyond its intended pharmacological action, chemotherapy can trigger immunogenic cell death. A multitude of clinical studies have drawn upon naturally occurring substances as foundational reservoirs of cancer-fighting drugs, notable examples being paclitaxel and vincristine. Even with these agents at hand for oncological care, chemotherapeutic setbacks are commonplace owing to dose-limiting toxic side effects and the onset of drug-tolerant phenotypes. The deployment of nanoscale delivery vehicles in this setting enables precise homing and delivery of selected drugs to neoplastic foci, thereby enhancing permeability and increasing intracellular accumulation of anti-cancer compounds [4].

Doxorubicin is a recognized therapeutic for leukemia that operates by triggering apoptotic pathways by introducing genetic lesions into malignantly altered cells. It achieves this by inserting itself between nucleotide bases, thereby generating reactive oxygen species (ROS) [5]. The burst of reactive oxygen species (ROS) elicited by doxorubicin constitutes the primary mechanism underlying its tumoricidal properties, positioning it as a potent weapon against neoplastic populations. Regrettably, its indiscriminate mode of action begets a spectrum of unwelcome toxicities, encompassing alopecia, profound tiredness, retching, nausea, and loose bowel movements [6]. Accordingly, there exists an imperative to supplant such agents with naturally derived substances that exhibit robust oncolytic potency.

Caffeine, an endogenously occurring trimethylxanthine, produces pronounced excitatory influences upon the human central nervous apparatus [7]. It promotes the outward transport of substances through efflux transporter systems under the regulatory control of the transcription factor Pap1, thereby streamlining the body's clearance mechanisms [8]. Caffeine has additionally garnered recognition for harboring tumor-suppressive capabilities; nonetheless, its abbreviated circulatory lifespan renders it unsuitable as a frontline pharmacological option [9]. Reports in the scientific literature highlight caffeine's aptitude for sabotaging DNA damage repair pathways within cancerous cells, thus amplifying their sensitivity to programmed death. It also disrupts the cell cycle machinery of malignant cells, triggering cell cycle arrest and halting the uncontrolled proliferation characteristic of cancer [8].

Nanotechnology continues to gain recognition as a domain of tremendous therapeutic potential, and particulate carriers formulated with caffeine exhibit considerable promise as a robust drug-delivery platform [10]. Nano-engineered constructs in the clinical arena are evolving rapidly to optimize pharmaceutical absorption and tissue-specific deposition, particularly through the use of mesoporous silica nanoparticles (MSNPs) [11].

Capitalizing on the inherent properties of both caffeine and MSNPs, we constructed caffeine-encased nanoparticles (CcNPs) as nanoscale therapeutics. We evaluated their efficacy against benzene-induced AML in rodent models through integrated computational, cell-based, and organism-level investigations targeting multiple anticancer biomarkers. Hematological profiling, renal and hepatic biomarker measurement, and elucidation of the implicated signaling routes collectively reinforce its standing as a viable therapeutic strategy.

Materials and Methods

Synthesis of mesoporous silica nanoparticles (MCM-41 generation)

Mesoporous silica nanoparticles were prepared via a wet-chemical synthesis route [12]. The alkalinity of deionized water (442 mL) was adjusted to pH 11 through the dropwise introduction of 29% ammonium hydroxide (Sigma-Aldrich Cat. No. 1336-21-6; EMSURE®, Darmstadt, Germany). The aqueous medium was brought to a temperature of 50 °C, after which 0.279 g of cetyltrimethylammonium bromide (CTAB) (Sigma-Aldrich Cat No. 57-09-0; Calbiochem®, Darmstadt, Germany) was incorporated under uninterrupted agitation. The pH was maintained at 10.3, and the mixture was allowed to return to ambient temperature. Subsequently, tetramethyl orthosilicate (TMOS, 1.394 mL) (Sigma-Aldrich Cat. No. 78-10-4; Darmstadt, Germany) was added with continuous stirring, and turbidity became apparent after 2 minutes. The reaction was stirred continuously overnight, after which it was filtered and rinsed with deionized water. The collected solid was desiccated at 90 °C and calcined at 500 °C for 5 h, affording a white product. This material was then finely pulverized into a powder. The dried powder was refluxed in methanol (100 mL) (Sigma-Aldrich Cat No. 67-56-1; Darmstadt, Germany) with concentrated HCl (1 mL) (Sigma-Aldrich Cat No. 7647-01-0; Darmstadt, Germany) for 24 hours at 50 °C to strip the CTAB porogen template. The resultant mesoporous silica nanoparticles (MSN) were harvested by filtration, exhaustively rinsed with water and methanol, and subsequently dried at 100 °C for 24 h.

Characterization of nanoparticles

The structural morphology and particulate dimensions of the mesoporous silica nanoparticles (MSNPs) were visualized by means of a field-emission scanning electron microscope (SEM, LEO SUPRA 55; Carl Zeiss AG, Oberkochen, Germany). For image acquisition, a small amount of the dry powdered material was mounted onto the SEM specimen holder using carbon adhesive film, and micrographs were recorded at an excitation voltage of 12 keV. The MSNPs were then subjected to additional physicochemical profiling by X-ray diffraction (XRD), ultraviolet-visible absorbance measurements, and Fourier-transform infrared spectroscopy. XRD patterns were collected on an X-ray spectrophotometer (Bucker D8 Advance, Karlsruhe, Germany), making use of Cu-Kά emission (λ = 1.54 °A), with the generator operated at 40 KV and a current of 30 mA. Nanoparticle diameter was calculated using the full width at half maximum (FWHM) of the diffraction peak inserted into the Debye-Scherrer equation (D = 0.9B/βCos) [13]. FTIR spectra were obtained by placing a fluidized sample preparation (400 µL) inside an FTIR spectrometer (Bruker, Tensor 27; Ettlingen, Germany), sweeping across the frequency domain of 400 to 4000 cm^{-1} with a spectral step size of 4 cm^{-1}. A UV-Vis spectrophotometer (Perkin Elmer UV/Vis–Lambda 25; Shelton, CT, USA) served to register the optical absorbance signatures of unmodified mesoporous silica nanoparticles (MSNPs), the neat pharmaceutical agent, and the therapeutic cargo-bearing nanoparticles. The absorbance data were gathered at ambient temperature over the wavelength interval of 250–800 nm.

Drug loading

To fabricate the active agent-loaded nanomedicine, 0.583 g of caffeine (Sigma Aldrich Cat. No. C0750-5G; ReagentPlus®, Darmstadt, Germany) was combined with normal saline (35 mL). This admixture was sonicated for 3 hours, after which MSNPs (145.75 mg) were added, and the resulting suspension was stirred overnight under constant mixing. The extent of cargo incorporation was computed according to an adapted version of the literature procedure [14]. Once the nanomedicine was prepared, a 1 mL fraction was centrifuged at 10,000 rpm for 10 min. Thereafter, the UV-Vis absorbance was measured at 209 nm.

Drug Loading = W1/W2 × 100; Encapsulation Efficiency = W2 − W3/W2 × 100.

(In these expressions, W1 stands for the caffeine mass contained within the nanomedicine, W2 signifies the total nanomedicine mass, and W3 is the mass of extract persisting in the supernatant). To improve the physiological availability of the nanoparticulate therapeutic, polyethylene glycol (PEG, 0.006 g) (Sigma-Adrich Cat No. 25322-68-3; BioUltra, Darmstadt, Germany) was solubilized in DMSO (4 mL) (Sigma-Adrich Cat No. 67-68-5; BioReagent, Darmstadt, Germany) to produce a polymeric matrix solution [15]. The blend was sonicated until complete PEG dissolution was achieved. Following this, the polymer-containing liquid was combined with the caffeine-bearing silica nanoparticles to a final volume of 35 mL and maintained under uninterrupted agitation for 2 hours [16].

Molecular docking studies

Computational fitting of the assembled nanomedicine (ligand) within the binding clefts of apoptosis-promoting markers (cFLIP-DISC complex, TRAIL-DR5 complex) and proliferation-suppressing markers (NFkB-p52/Rel B/DNA complex) was carried out using the PyRx software suite (v.0.8) (accessed on 18 February 2020) [17] in conjunction with Autodock Vina (v.1.2.5) [18]. The ligand's conformational energy underwent minimization through the Autodock engine, and the resulting macromolecule–ligand interaction patterns matched the interaction energies anticipated from quantum chemical computations [19]. The docking-derived affinity scores were inspected to reflect the magnitude of intermolecular association between the ligand and the receptor proteins under investigation. Furthermore, BIOVIA Discovery Studio (v. 4.5) [20] was used to map the two- and three-dimensional arrangements of contacts involving amino acid functional groups.

Cytotoxicity assay

To identify the most appropriate dosage windows for the test compounds, a brine shrimp lethality assay was conducted. Briefly, brine shrimp cysts were incubated in a saline enrichment medium until nauplii emerged. Under a stereomicroscope, batches of fifteen larvae were manually counted and distributed into serially diluted test solutions for a 24-hour challenge period. Every dilution level was assayed in triplicate, with distilled water serving as the untreated reference. The concentration that elicited mortality in 50% of organisms (LC50) at the 24-hour endpoint was extrapolated using probit analysis [21].

In vitro bioassays

Free radical-neutralizing performance was gauged through a panel of complementary test systems. Total antioxidant capacity was quantified using the phosphomolybdenum method [22], with minor procedural adjustments. Similarly, total reducing power and DPPH radical decolorization assays were performed according to the experimental protocols published by Moein *et al*. [23].

In vivo bioassays

Pain-suppressing capability across the different treatment groups was measured using the hot plate paradigm [24]. The anti-coagulation assay, which quantifies the time required for blood to clot in the absence of an externally added trigger, was performed as previously described [25]. An intraperitoneal bolus was delivered to each mouse cohort, and the first time point was captured immediately upon injection. To this end, the tails of the animals were first disinfected with ethanol, and subsequently, a 1–2 mm portion was snipped from the terminal end using a sanitized surgical scissors. Gentle compression along the tail expressed a generous blood droplet, which was transferred onto a pristine glass microscope slide. The blood sample was monitored by maneuvering a toothpick through the droplet in a repetitive circular path until a visible fibrin filament materialized. The time elapsed to fibrin strand emergence, a marker of coagulation, was measured with a stopwatch. A subsequent reading was obtained at 3 hours post-administration, and the results were then interpreted. DMSO (0.1%) served as the negative control, whereas aspirin (1 mg/kg) served as the positive reference standard. Concurrently, mood-elevating activity was assessed using the classic tail suspension procedure described by Xu *et al*. [26].

Experiment design and sprague-dawley model

Ethical sanction for the investigation was granted by the Institutional Review Board of Quaid-i-Azam University, as documented in Approval Letter No. #BEC-FBS-QAU2020-221. A shipment of forty female Sprague-Dawley rats was sourced from the National Institute of Health (NIH), Islamabad, and subsequently partitioned into eight separate experimental arms, each receiving a distinct interventional protocol, as itemized here: Group (1) untreated control (saline vehicle); Group (2) benzene challenge exclusively; Group (3) doxorubicin together with benzene; Group (4) caffeine together with benzene; Group (5) MSNPs together with benzene; Group (6) CcNPs together with benzene; Group (7) caffeine paired with doxorubicin plus benzene; Group (8) CcNPs paired with doxorubicin plus benzene. A settling-in interval of seven days was allotted, and the colony was accommodated within the Primate Facility of Quaid-i-Azam University, maintained under a regular 12-hour photoperiod regime with continuous free access to hydration and pelleted rodent feed.

Benzene dosing mixtures were readied by emulsifying benzene (Sigma Aldrich Cat. No. 71-43-20; Darmstadt, Germany) together with normal saline, preserving a volumetric proportion of 1:3. An aliquot of the benzene admixture (200 µL) was infused into the caudal vein of animals belonging to groups 2 through 8 on alternating days spanning a two-week window to precipitate leukemogenesis, with subsequent corroboration of AML onset.

Doxorubicin (a 10 mg vial rehydrated using 5 mL of normal saline), an anthracycline cytotoxic agent, was procured from Actavis, Italy (Cat. No. 25316-40-9), from which a mother solution of 3.75 mg/1.8 mL was constituted. After the 14 intravenous benzene instillations, a fixed doxorubicin dosage (0.625 mg/0.3 mL) was administered to the animals in groups 3, 7, and 8 every other day for 3 weeks.

A mother liquor of caffeine (Cat. No. C0750-5G) was produced by dissolving 0.583 g of caffeine into normal saline (35 mL). Following verification of leukemic engraftment, the mother liquor was delivered intravenously (0.3 mL per subject) to rats in groups 4 and 7 for a period spanning three uninterrupted weeks (8 mg/kg).

In parallel, caffeine-enveloped nanoparticles (CcNPs) were administered via intraperitoneal injection (0.3 mL per subject) to rats assigned to groups 6 and 8 on every other day for 3 weeks. Apart from the MSNP vehicle (group 5) and the caffeine-enveloped nanoparticles (CcNPs, groups 6 and 8), all other administered agents—namely caffeine and doxorubicin—were furnished as unbound, non-encapsulated drugs.

Once the prescribed courses of treatment were concluded, all rodent subjects were humanely euthanized and subjected to necropsy in alignment with the standards prescribed by the Guide for the Care and Use of Laboratory Animals [27].

Morphological analysis

Peripheral blood smears on glass slides were prepared promptly post-necropsy and processed with Giemsa stain to permit cytomorphological assessment. The film-bearing slides were first desiccated at room temperature, after which the staining solution was layered dropwise and incubated for 10 minutes. The dyed slides were subsequently

rinsed under a gentle stream of tap water and allowed to air-dry once more before being examined under light microscopy [28].

Blood profiling

A comprehensive hematological panel (CP) was generated through the use of a Z3 automated hematology analyzer (Zybio Inc., Shenzhen, China) at the Islamabad Diagnostic Centre (IDC), Pakistan, yielding quantitative data on hemoglobin (HGB), thrombocyte counts (PLT), erythrocyte numbers (RBC), leukocyte numbers (WBC), as well as supplementary hematometric indices. For the biochemical determination of hepatic and renal enzyme activities, a Micro Lab 300 auto-analyzer (Merk, Darmstadt, Germany) was brought into service. The enzymatic parameters quantified included alkaline phosphatase (ALP), alanine aminotransferase (ALT), aspartate aminotransferase (AST), and creatinine, all measured via commercially supplied analytical kits (AMP diagnostic kits).

mRNA extraction

For the purpose of conducting relative transcript quantification through real-time PCR, messenger RNA was harvested from hepatic tissue specimens. Briefly, cryogenically stored tissue pieces weighing 10 mg each were excised and mechanically disrupted in 1 mL of TRIZOL solution (Sigma-Aldrich Cat No. 136426-54-5; Darmstadt, Germany). The resulting lysate was further processed according to the extraction workflow established by Chomczynski and associates [29]. The purified RNA product was then subjected to spectrophotometric quantitation on a NanoDrop™ 2000/2000c device (Cat. No: ND-2000; Waltham, MA, USA), and its molecular integrity was verified through electrophoretic separation on a 1% agarose matrix.

cDNA synthesis

The purified messenger RNA fractions were subsequently converted into complementary DNA using a reverse transcription kit (cDSK01-050, VIVANTIS, Shah Alam, Malaysia). To authenticate the success of the cDNA generation step, conventional PCR was performed according to the manufacturer's protocol, allowing verification of suitable primer annealing temperatures and confirmation of cDNA integrity. The specific amplification of the intended transcript was performed by pipetting the reaction mixture components into 200 µL PCR tubes (Axygen, Union City, CA, USA). Once amplification was complete, the reaction products were separated by electrophoresis on a 2% agarose gel containing ethidium bromide for visualization [30]. Amplicons corresponding to the expected fragment lengths were then duly validated.

RT PCR expression analysis

To measure relative transcript levels and quantify amplified cDNA, a MIC qPCR instrument from BioMolecular Sciences (Sydney, Australia) was brought into service. The DNA-binding fluorophore EvaGreen® Master mix (Biotium, Inc., Fremont, CA, USA) served as the detection chemistry throughout the assay. A curated panel of gene targets was subjected to expression profiling, comprising:

• STMN1 (F-TTGCCAGTGGATTGTGTAGAG, R-TTCTTTTGATCGAGGGCTGAG),
• P53 (F-TCCGACTATACCACTATCCACTAC, R-GCACAAACACGAACCTCAAAG),
• GAPDH (F-TCCAGTATGACTCTACCCACG, R-CACGACATACTCAGCACCAG),
• mTOR (F-AGTGAAAGTGAAGCCGAGAG), (R-CGACAAGGAGATAGAACGGAAG),
• Rel A (F-CTACGAGACCTTCAAGAGCATC, R-GATGTTGAAAAGGCATAGGGC),
• Rel B (F-CTTTTCTCAAGCTGACGTGC, R-AGATCTCCAGGTCCTCGTATG),
• DR5 (F-TCAACCCTGTGCCAATCC, R-ATGAACTCCTTCCAGCGTG),
• cFLIP (F-AGAAGCCCTCACCTTGTTTC, R-CTCTTGTCCTTGGCTACCTTG),
• TRAIL ligand (F-CACATTACCGGGATCACTCG, R-AGCTCTCCGTTTCTCAAGTG),
• and Cyt-c (F-CCCTAAGAGTCTGATCCTTTGTG, R-TCCAGTCTTATGCTTGCCTC).

Normalized fold-change values for gene expression were calculated according to the mathematical framework established by Pfaffl. Data processing was handled using the Relative Expression Software Tool (REST-384, version 2 beta v.2, 2006), which calculates relative expression ratios in real-time PCR using a pairwise fixed reallocation randomization test. A melt curve analysis was appended at the final stage to screen for any unintended amplification products. The observation of a solitary, sharply defined peak in the q-PCR melt curve confirmed the absence of primer-dimer formation or non-specific amplification artifacts.

Statistical analysis

Summary statistics were tabulated using GraphPad Prism software (version 5.01, 2007; Boston, MA, USA), and all data are presented as the mean ± standard error of the mean (SEM). A predetermined threshold for statistical significance was set, with any computed p-value < 0.05 deemed to represent a statistically reliable difference (< 0.05, < 0.01, or < 0.001). Comparisons across multiple groups were conducted using a one-way analysis of variance (ANOVA), supplemented by Tukey's post hoc test for detailed intergroup comparisons.

Results and Discussion

Characterization of MSNPs and drug loading

Micrographs captured via scanning electron microscopy displayed evenly scattered spherical MSNPs featuring an average size of 120 nm. The X-ray diffractogram authenticated the formation of MSNPs, evidenced by a distinctive diffraction peak at $2\theta = 29.18$, corresponding to MSNPs with a calculated dimension of 118.18 nm. FTIR spectral tracing showed characteristic vibrational bands in the nanomedicine that coincide with those of caffeine, indicating successful envelopment of the particles with caffeine molecules. UV-Vis spectroscopic absorbance traces recorded for free caffeine, the nanomedicine, and bare MSNPs validated the integration of caffeine onto the nanoparticulate scaffold, achieving a cargo incorporation efficiency of 28%.

Nanomedicine exhibiting strong interaction with pro-apoptotic TRAIL-DR5 complex

The recognition cavity of the TRAIL-DR5 protein underwent molecular docking against the caffeine assembled in its nano-vehicle configuration (ligand) (pdb:1du3), as represented in **Figure 1a**. The energetically most favorable conformational solution showed a binding affinity of −6.8 and an RMSD of 0.00 when processed with PyRx. Follow-up dissection using BIOVIA Discovery Studio revealed hydrogen bonds, nonpolar interactions, and Van der Waals interactions. Most remarkably, canonical hydrogen-bond linkages were mapped between the ligand and the receptor-side-chain ASN228. In addition, four carbon–hydrogen bridges were cataloged connecting the ligand to residues ASN228, SER229, and TYR240. A pair of pi–sulfur contacts mediated by amino acid CYS230 was also recorded. Interspersed among five hydrophobic connections were two pi–pi face-to-face stacks, two pi–pi T-shaped geometries engaging TYR240, and one pi–alkyl bond tethering ARG227. Numerous amino acid positions further participated in Van der Waals-type associations.

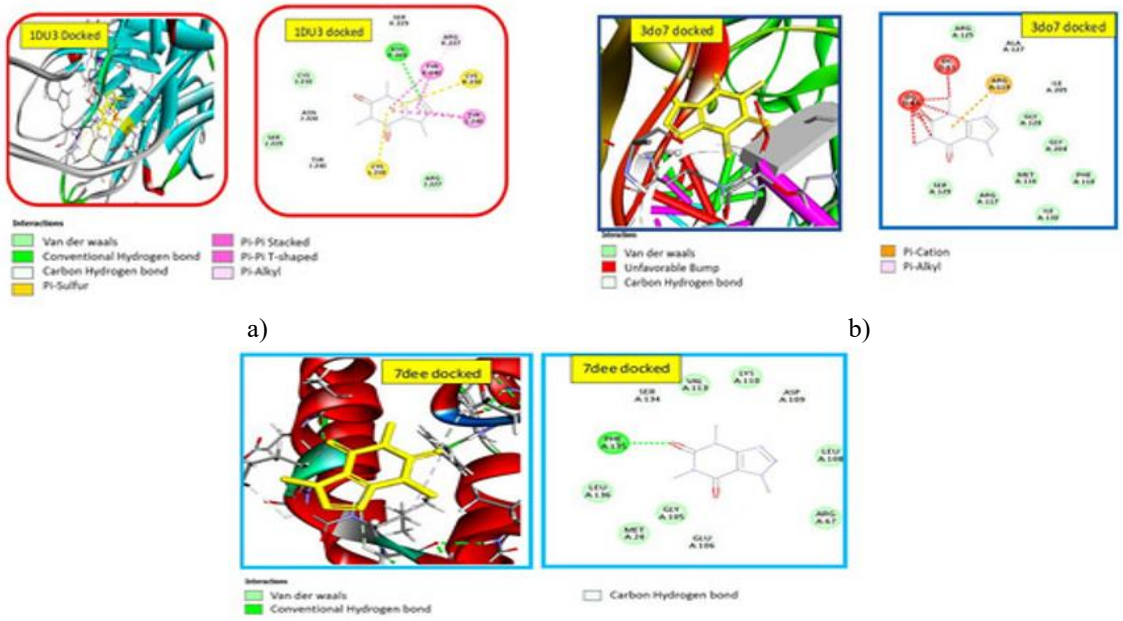

Figure 1. Molecular docking between ligand and (a) TRAIL-DR5 complex (PDB:1du3), (b) NFκB p52/RelB/DNA protein complex (PDB:3do7), (c) cFLIP-DISC complex (PDB:7dee), proposing strong binding affinities with anti-leukemic markers.

Docking studies confirmed the strong binding efficiency of the ligand with anti-proliferative NF-kB p52/RelB/DNA complex

The energetic favorability computed for caffeine at the intermolecular contact surface of the NF-kB p52/RelB/DNA complex protein amounted to −5.6 Kcal/mol, with an attendant RMSD of 0.00, signifying exceptional associative strength and molecular interplay, as conveyed in **Figure 1b**. A more exhaustive exploration of this top-ranked conformation, conducted in BIOVIA Discovery Studio (version 2021), revealed van der Waals forces, nonpolar interactions, and hydrogen-bridging. Engagements were also discerned with the DNA constituent embedded within the multiprotein architecture. Most conspicuously, a notable interplay was distinguished involving the residue ARG:119. These theoretical simulations revealed nanomedicine's capacity to interact with both death-inducing and growth-restraining macromolecular assemblies, a finding subsequently validated by cell-based and whole-animal studies.

Nanomedicine exhibiting strong interaction with c-FLIP

The ligand was seated within the enzymatically active region of c-FLIP (pdb:7dee), illustrated in **Figure 1c**. A resulting binding affinity measurement of −5.3 and an RMSD value of 0.00 were obtained. Beyond Van der Waals-type interactions, carbon–hydrogen bridges and conventional carbon–hydrogen linkages were observed with amino acid functional groups.

Increased antioxidant potential of caffeine in the form of nanomedicine

The total reducing power evaluation revealed statistically significant ($P < 0.001$) reductive activity across all therapeutic arms assessed. A notable observation was that the electron-donating capacity of caffeine underwent amplification ($P < 0.05$) when dispensed in the nano-formulated format, as detailed in **Figure 2a.** The total antioxidant capacity measurement mirrored this general pattern. Strikingly, co-administration of the nanomedicine with the drug boosted ($P < 0.001$) the radical-quenching performance by 16.5% compared with the drug delivered in isolation **(Figure 2b).** Correspondingly, the DPPH radical-scavenging test confirmed a 24.8% increase ($P < 0.05$) in the antioxidative strength of caffeine when delivered as a nanoparticulate medicine **(Figure 2c).**

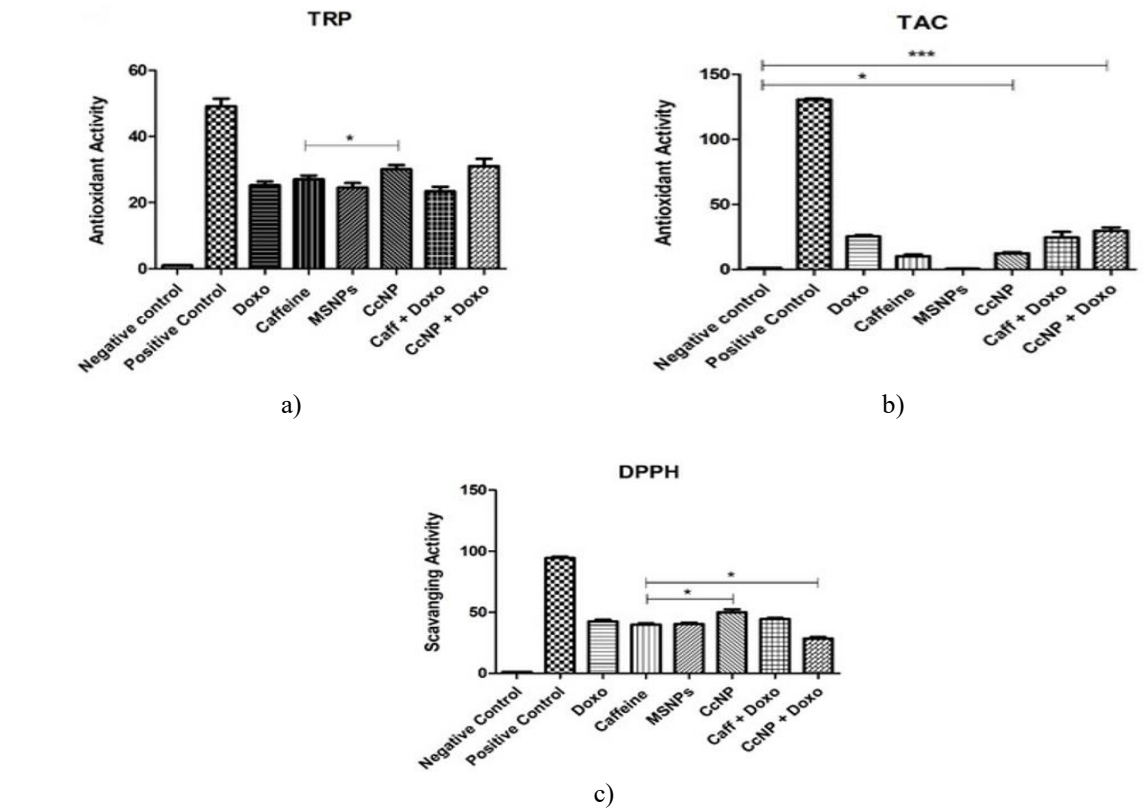

Figure 2. Antioxidant potential analysis of different treatment groups via (a) total reducing power assay, (b) total antioxidant capacity, and (c) 2,2-diphenyl-1-picrylhydrazyl (DPPH) assay. All treated groups exhibit

significant antioxidant potential, especially the CcNP-treated group. Statistical significance levels are defined as = P < 0.05; = P < 0.001.

Enhanced biological potential of nanomedicine as anti-depressant, analgesic, and anti-coagulation agent in rat models

When the nano-formulation is administered alongside standard chemotherapy, a discernible attenuation (P < 0.01) of the cytotoxic burden is observed, as measured by the brine shrimp lethality assay **(Figure 3a).** Furthermore, the co-treatment protocol yields pronounced elevations in three distinct pharmacological dimensions—namely, mood-elevating capacity (15.3%), pain-relieving action (88%), and clot-inhibiting ability (16%)—attributable to the nano-encapsulated agent (P < 0.001) relative to doxorubicin alone. These data collectively affirm the robust in vivo bioactivity of the nanomedicine in Sprague-Dawley rats **(Figure 3b–3d).**

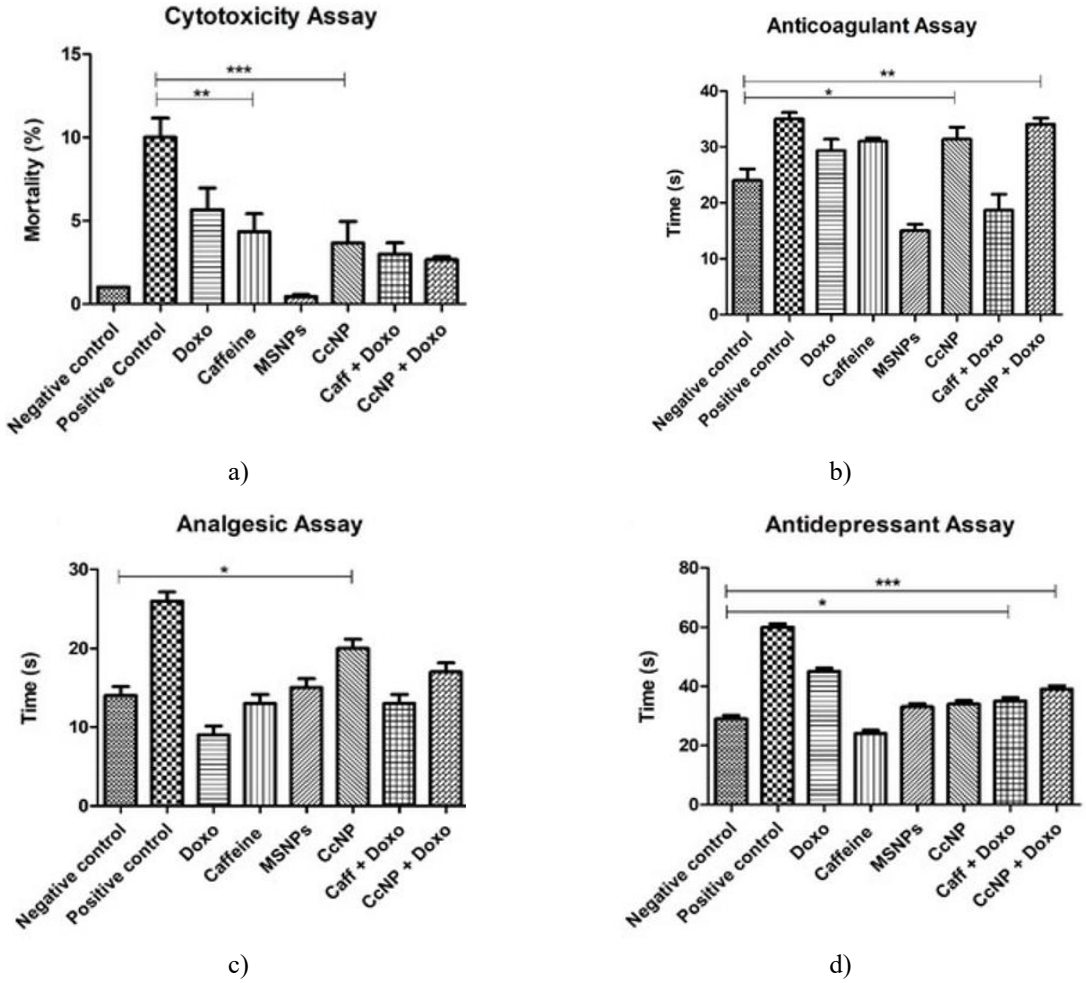

Figure 3. Analysis of the biological potential of different treatment regimes: (a) Brine shrimp assay exhibits reduced toxicity of nanomedicine (P < 0.05) as compared to chemotherapy, (b) The anti-coagulation potential of chemotherapy significantly increased (P < 0.01) when combined with nanomedicine, (c) The analgesic potential of caffeine significantly increased (P < 0.05) when used as nanomedicine, and (d) Nanomedicine exhibited significantly increased (P < 0.05) anti-depressant potential as compared to caffeine. Statistical significance levels are defined as P < 0.05, P < 0.01, and P < 0.001, respectively.

Restoration of liver, heart, and kidney weights back to normal after CcNP Treatment

Relative organ mass quantification revealed a measurable swelling of hepatic (P < 0.05), cardiac (P < 0.001), and renal (P < 0.05) tissues in the benzene-exposed experimental. Upon intervention with the nanoparticulate therapeutic (CcNPs), the masses of these organs contracted (P < 0.05) and fell into ranges indistinguishable from those characterizing the healthy control group. Equivalent restorative trends were noted in the arms dosed with bare MSNPs, doxorubicin as a single agent, and the joint administration of CcNPs with doxorubicin.

Restoration of blood parameters upon nanomedicine administration

Cytomorphological assessment uncovered both an overproduction of erythrocytes and the circulation of immature blast forms in the leukemic rats exposed to benzene. The nano-formulation reversed these abnormalities, reinstating structurally sound red blood cells and a well-proportioned nucleus-to-cytoplasm relationship among the treated cohorts. A complete hemogram panel revealed a pathological spike in total leukocyte count, accompanied by a precipitous decline in erythrocyte count, in the benzene-challenged group ($P < 0.05$). Regarding white cell counts, the dual-modality regimen statistically outperformed nanomedicine monotherapy, with the CcNP–doxorubicin pairing standing out as particularly efficacious **(Figure 4a).**

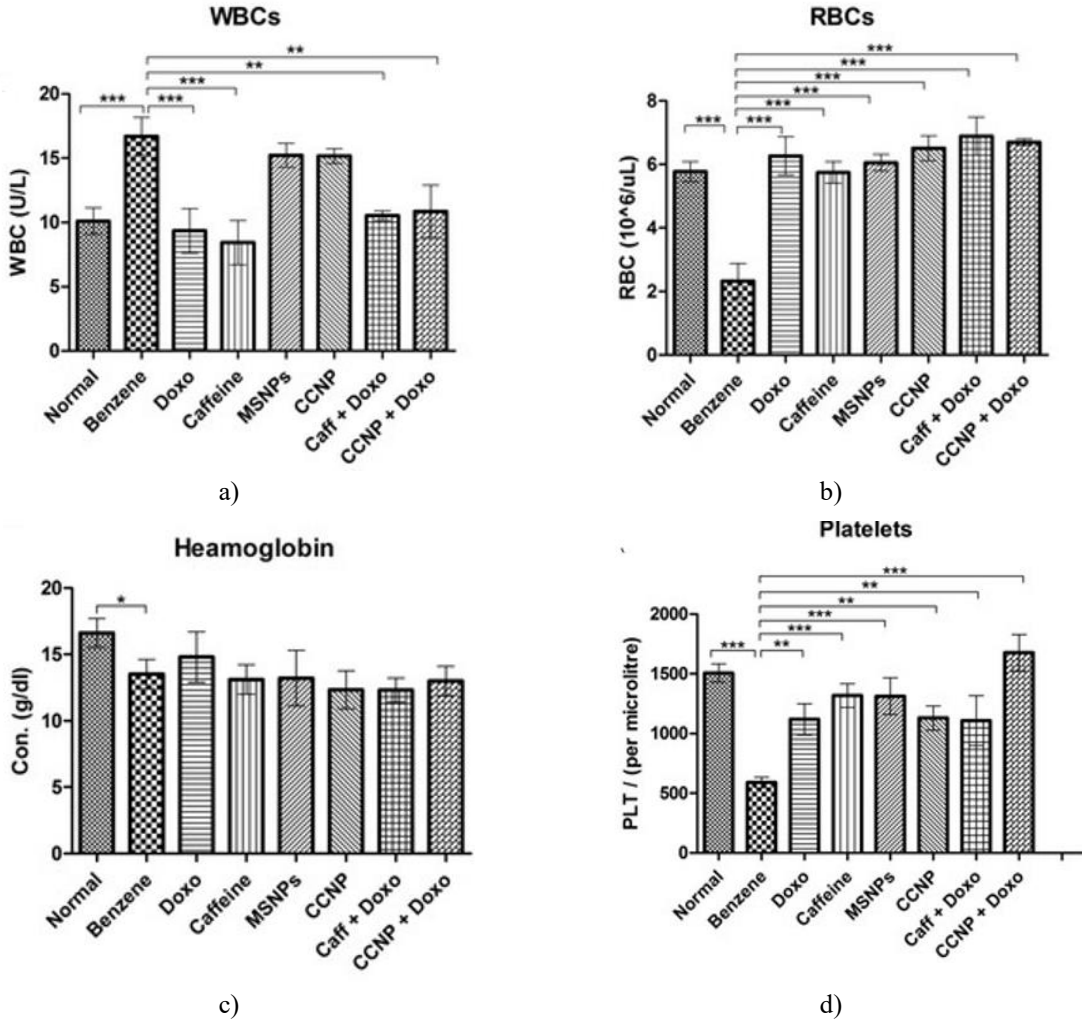

Figure 4. Blood parameters of different experimental groups: (a) Total white blood cells count, (b) red blood cells, (c) hemoglobin, and (d) total platelets count. The values are shown as mean ± SEM. The intergroup comparisons were made using one-way ANOVA with Tukey's post hoc test. Statistical significance levels are defined as $P < 0.05$, $P < 0.01$, and $P < 0.001$.

Absolute counts of monocytes, eosinophils, neutrophils, and lymphocytes likewise increased to anomalous levels in the leukemic animals. The nano-therapy had a beneficial effect on them, though these shifts did not reach statistical significance. In parallel, erythrocyte numbers were normalized after the course of nanomedicine delivery **(Figure 3b).** Both hemoglobin concentrations and platelet counts decreased in the diseased cohort ($P < 0.05$); the interventions exerted no meaningful effect on hemoglobin status, whereas platelet counts recovered substantially ($P < 0.05$) among the treated subjects, with heterogeneity in the magnitude of the response **(Figures 4c and 4d).**

Enzymatic activities normalized after drug treatment

Hepatocellular biomarker profiling revealed suppression of ALP ($P < 0.001$) and elevations of ALT and AST ($P < 0.001$) in benzene-intoxicated rats; these pathologic shifts were normalized to homeostatic baselines with nanomedicine administration. More precisely, ALP readings rose markedly ($P < 0.001$), while ALT and AST fell sharply ($P < 0.001$) in the wake of nano-treatment. The alternative therapeutic protocols also produced encouraging patterns, though with variable potency **(Figures 5a–5c).** The nanomedicine successfully normalized creatinine concentrations ($P < 0.01$), which had been significantly pushed above the physiological ceiling in the benzene-exposed subjects ($P < 0.05$), a finding indicative of renal functional compromise. The combined treatment schedules yielded even superior restoration of kidney performance parameters **(Figure 5d).**

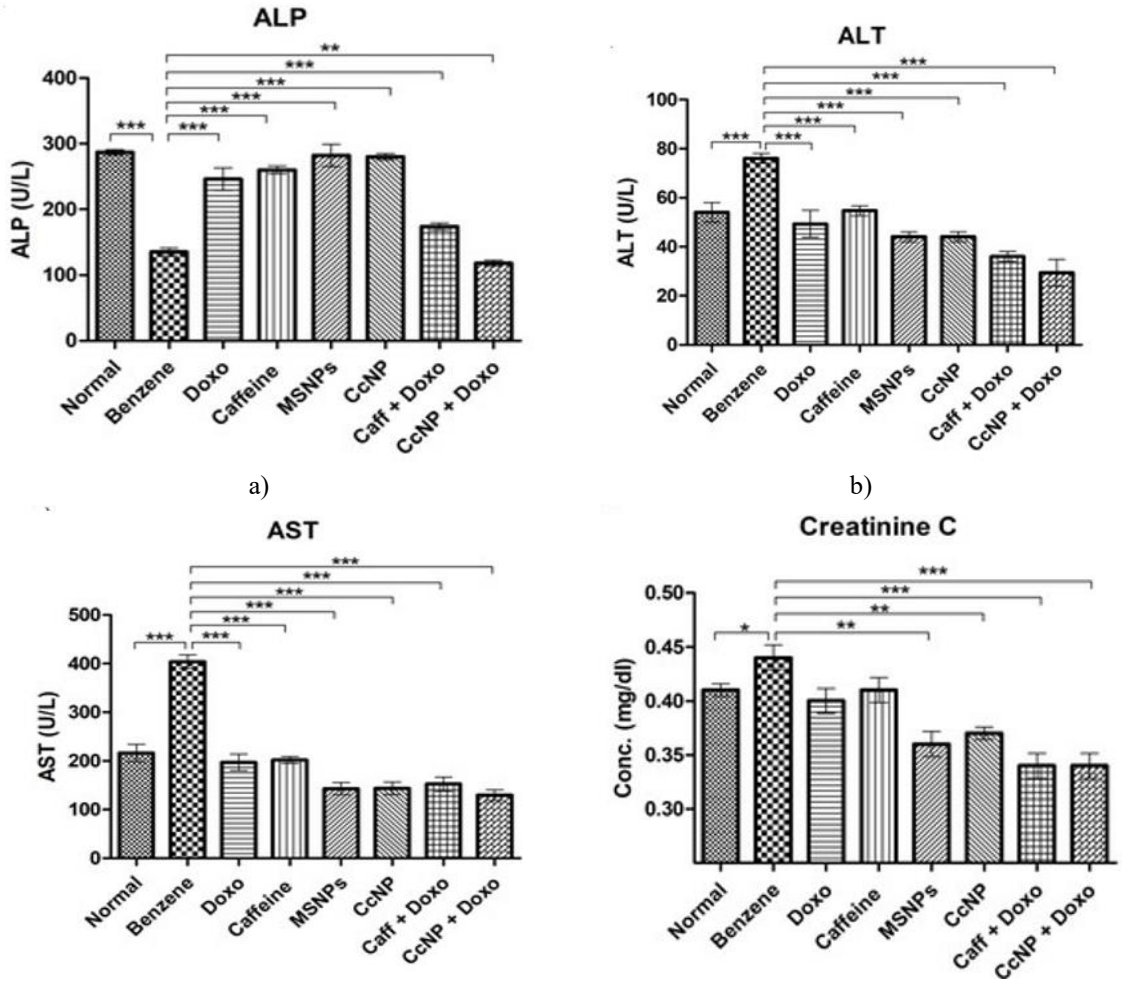

Figure 5. Levels of hepatic and renal biomarkers among various experimental groups: (a–d) exhibit the mean + SEM values of ALP, ALT, AST, and creatinine, respectively. The intergroup comparisons were made using one-way ANOVA with Tukey's post hoc test. Statistical significance levels are defined as $P < 0.05$, $P < 0.01$, and $P < 0.001$.

Suppression of STMN1 expression by nanomedicine

A molecular fingerprint of acute myeloid leukemia (AML) is the marked transcriptional upswing of the STMN1 locus, a gene that serves as a diagnostic biomarker for this hematologic malignancy. The benzene-exposed experimental arm registered a striking elevation in STMN1 messenger levels ($P < 0.001$), corroborating the successful establishment of the leukemic state. Conversely, exposure to the nano-engineered formulation provoked a dramatic suppression of STMN1 transcriptional activity ($P < 0.001$) **(Figure 6a).**

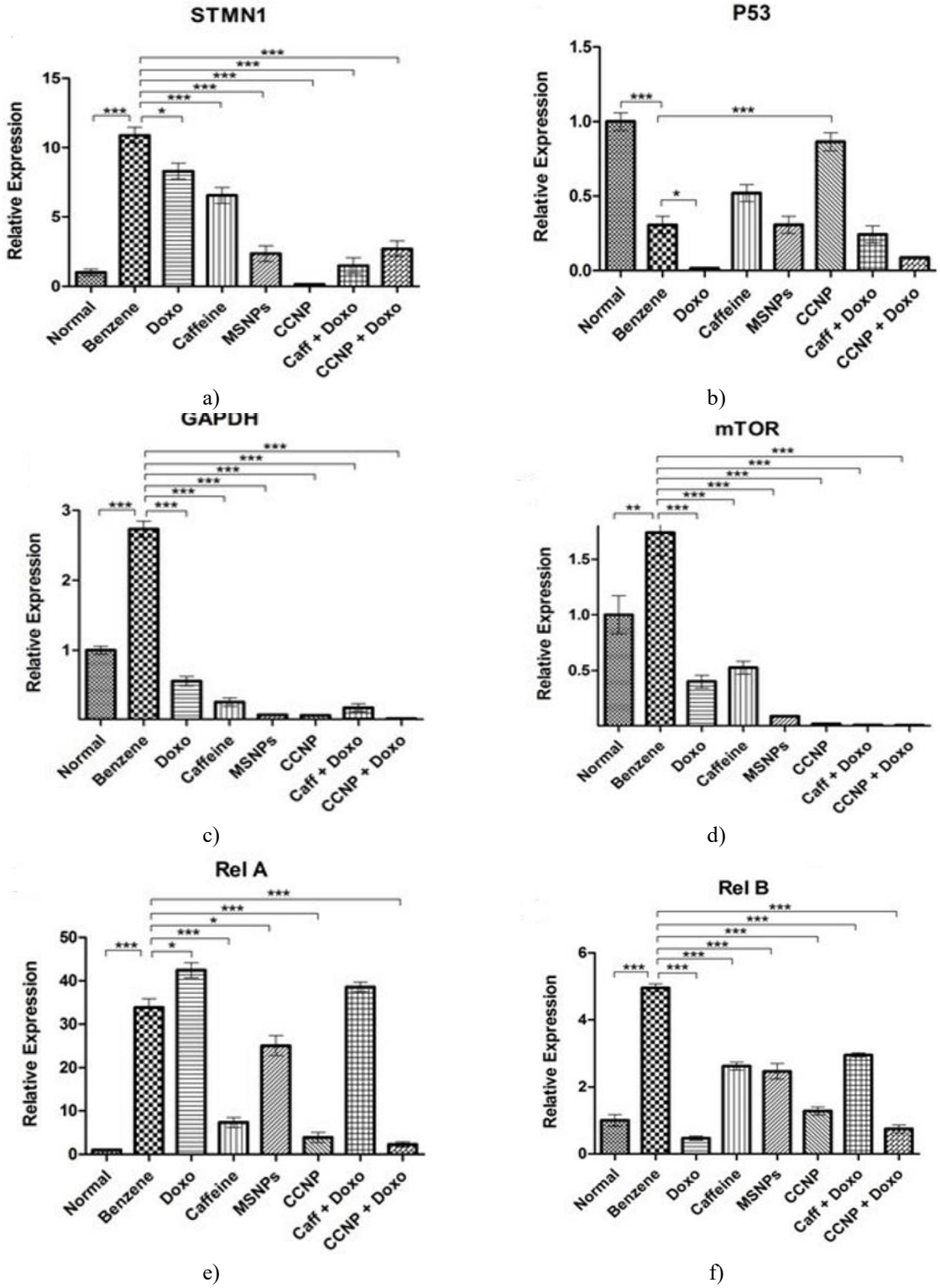

Figure 6. Gene expression analysis of molecular markers among various experimental groups: (a) depicts AML induction via assessment of STMN1, (b) exhibits the tumor suppressor gene P53, (c, d) reveal GAPDH and mTOR expression, (e, f) represent NF-kappaB pathway markers Rel A and Rel B. The values are shown as mean ± SEM. The intergroup comparisons were made using one-way ANOVA with Tukey's post hoc test. Statistical significance levels are defined as $P < 0.05$, $P < 0.01$, and $P < 0.001$.

Upregulation of tumor suppressor gene p53 by nanomedicine

Universally acknowledged as the guardian of chromosomal stability, the p53 tumor suppressor protein primarily executes genome-protective functions, and its transcriptional silencing is commonly associated with malignant progression. The inherent p53 expression signature was recovered following application of the nano-therapeutic

agent ($P < 0.001$), rebounding from the downswing triggered by AML induction in our rodent leukemia paradigm **(Figure 6b).**

Regulation of glycolysis by nanomedicine in leukemic rats

The glycolytic enzyme GAPDH (Glyceraldehyde-3-phosphate dehydrogenase), which catalyzes a rate-limiting reaction in step 6 of the pathway, serves as a surrogate indicator of cellular bioenergetic output. The benzene challenge led to a steep increase in GAPDH transcript abundance, a signature of runaway energy metabolism that fuels malignant expansion. The nanomedicine, by contrast, substantially reduced GAPDH expression to constitutive levels ($P < 0.001$). Unformulated caffeine, doxorubicin, and the various combinatorial treatment designs similarly demonstrated beneficial modulatory effects **(Figure 6c).**

Regulation of the mTOR pathway by nanomedicine

The serine/threonine kinase mTOR operates as a central regulatory hub governing gene transcription, cellular hypertrophy, proliferative drive, and survival signaling. Benzene insult elicited a pronounced escalation in mTOR transcriptional output, yet this surge was substantially blunted ($P < 0.001$) upon dosing with the nano-formulation. Pharmacological pairings incorporating the chemotherapeutic backbone also imparted robust benefit ($P < 0.001$), as illustrated in **Figure 6d.**

Nanomedicine induces anti-proliferative effects through NF-kappa B pathway inhibition

A dominant signaling cascade that controls somatic cell expansion in acute myeloid leukemia is the NF-kappaB signaling pathway. Transcript levels of the NF-kappa B pathway archetypal effectors Rel-A and Rel-B were elevated in the leukemic cohort, reflecting unbridled hyperproliferation. Subjection to the nano-carried drug, both as monotherapy and in concert with doxorubicin, markedly diminished Rel-A expression ($P < 0.001$). In parallel, Rel-B transcript concentrations were significantly reduced by doxorubicin, the nanomedicine, and their combined use ($P < 0.001$), findings that collectively indicate a shutdown of the non-canonical branch of the pathway **(Figures 6e and 6f).**

Regulation of the TRAIL pathway by CcNP

Exposure to benzene suppresses the transcriptional output of death receptor 5 (DR5) while simultaneously boosting the levels of the inhibitory regulator FLIP, both of which hold pivotal roles in governing apoptotic signaling through the extrinsic TNF-related apoptosis-inducing ligand (TRAIL) axis. Our findings indicate that CcNP not only reinstated DR5 transcript abundance ($P < 0.001$) but also acted in concert with standard chemotherapy to enhance its expression ($P < 0.001$). Moreover, CcNP reduced cFLIP expression ($P < 0.001$), thereby disinhibiting the cell death machinery **(Figures 7a and 7b).** The benzene challenge led to a marked upswing in TRAIL ligand transcription ($P < 0.001$); however, the nano-formulation returned these levels to the physiological baseline **(Figure 7c).** Cytochrome c concentrations rose following benzene administration, a phenomenon plausibly stemming from mitochondrial outer membrane compromise within the malignant hematopoietic cells **(Figure 7d).** These elevated values were substantially normalized by several pharmacological protocols, including the nanomedicine arm ($P < 0.001$). It should be noted, however, that the nano-formulation did not produce a measurable impact on the transcriptional profiles of caspases 3, 7, 8, and 9.

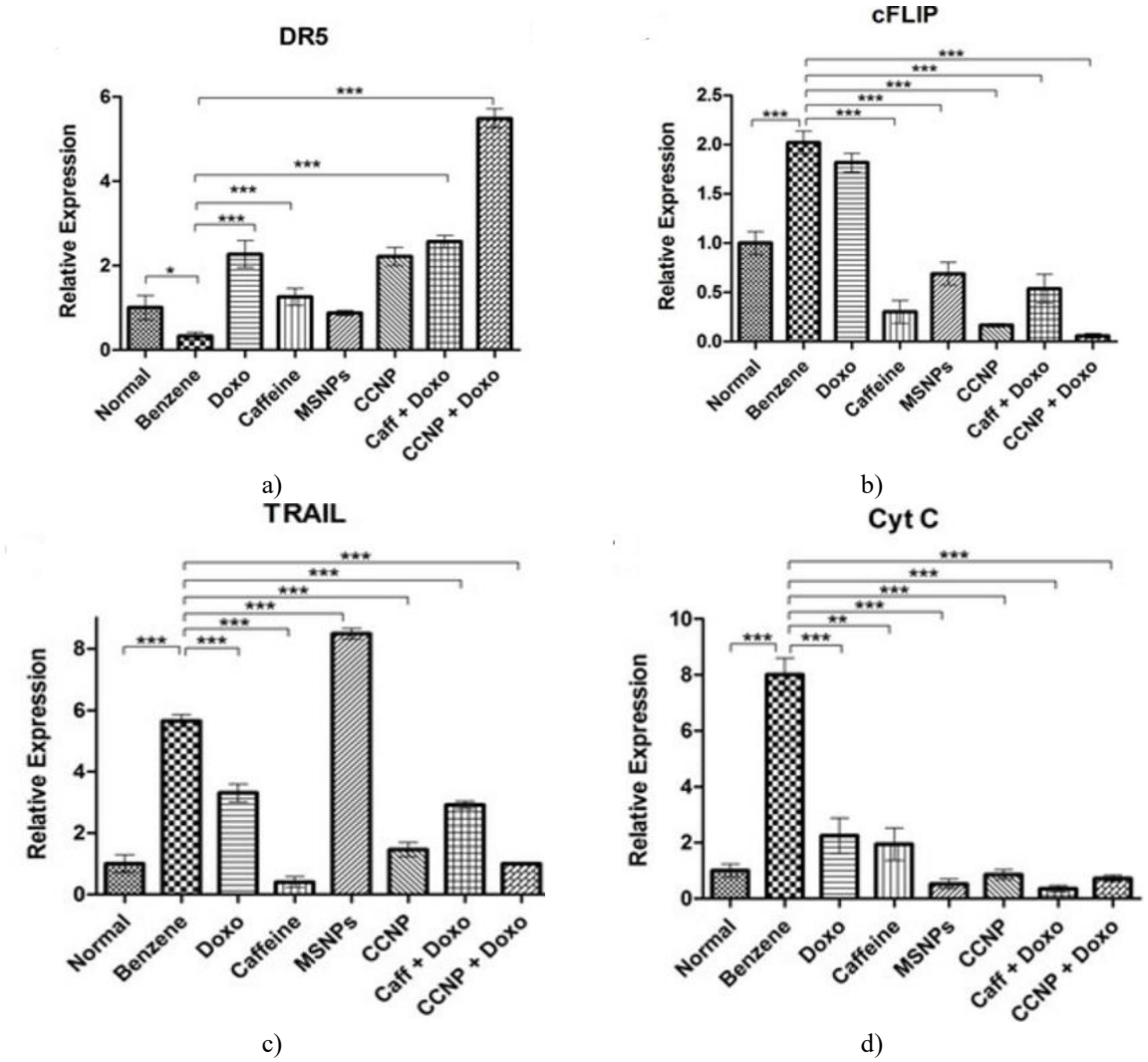

Figure 7. Relative gene expression of TRAIL pathway components, including death receptor 5 (a), FLICE-like inhibitory protein (b), TRAIL ligand (c), and cytochrome-c (d). The values are shown as mean ± SEM. The intergroup comparisons were made using one-way ANOVA with Tukey's post hoc test. Statistical significance levels are defined as $P < 0.05$, $P < 0.01$, and $P < 0.001$.

Nanoscale particles are increasingly used as pharmaceutical carriers owing to their ability to cross both the blood–brain barrier and cellular membrane barriers, thereby circumventing the principal challenge of achieving anatomically precise delivery while minimizing collateral toxicities [31]. In the present investigation, scanning electron microscopy validated the hollow, spherical architecture of the MSNPs alongside their dimensional characteristics. X-ray diffractometry further corroborated the particle size and geometry, findings that align with previously reported datasets [32]. The diffraction signals attributable to MSNPs confirmed the presence of SiO_2 and supported earlier published accounts [33]. Both Fourier-transform infrared spectroscopy and ultraviolet-visible absorption analyses generated concordant results, substantiating the effective surface deposition of caffeine onto the MSNP carriers [34].

Computational docking simulations were undertaken to probe the interplay between the nanomedicine and the catalytic pockets of the designated protein targets and macromolecular assemblies. Given that FTIR spectral data verified the presence of caffeine decorating the exterior of the nanoparticulate entities, its contacts with active-site amino acid side chains were evaluated employing caffeine as the molecular probe. Earlier published work has documented that quinacrine (QC), a recognized ligand, triggers apoptotic cell death by influencing both the TRAIL-DR5 supramolecular assembly and the mitochondrial intrinsic cascade [35]. The binding energetics and intermolecular contacts of QC and caffeine were juxtaposed. The calculated affinity scores amounted to −6.5 for QC and −6.8 for caffeine. The engagement profile of caffeine with the receptor's binding cleft encompassed a greater number of hydrogen bridges relative to QC.

Furthermore, QC positions itself at the periphery of the protein assembly, forming a ternary complex with TRAIL and DR5. Caffeine likewise binds to the protein architecture, forming a caffeine-TRAIL-DR5 complex. Similarly, caffeine formed robust hydrogen-bonding interactions with the TRAIL-DR5 complex, attributable to its outwardly oriented hydrophilic moieties. The Van der Waals-type forces detected arose from the nonpolar alkyl termini of the caffeine molecule. In contrast, the pi–pi stacked and pi–pi T-shaped configurations originated from the aromatic ring systems of the ligand. The multiplicity of hydrogen-bonded connections implies that caffeine serves as an enhancer of TRAIL-DR5 complex assembly. These extensive intermolecular associations between caffeine and the protein scaffold are compatible with the notion that the CcNP-TRAIL-DR5 assembly exhibits markedly greater stability than the QC-TRAIL-DR5 counterpart.

Another molecular target evaluated, namely the p52:RelB:kB DNA complex, shows that the DNA backbone adopts an asymmetric conformation upon direct contact with the protein component via ARG 125. Prior in vitro binding analyses and cellular reporter gene assays have demonstrated that the presence of Arg 125 within the p52:RelB heterodimer is essential for DNA engagement and the subsequent transcriptional activation at selective kB motifs, although not universally across all such sites [36]. Our docking simulations reveal the engagement of both ARG 119 and ARG 125 with caffeine, a molecular arrangement that generates steric clashes with the DNA at the ligand's docking site. Consequently, caffeine in its nano-formulated state behaves as a competitive antagonist, corroborating the suppressive action of the ligand (caffeine) and thereby obstructing the assembly of the functional complex.

The cellular FLICE-like inhibitory protein (c-FLIP), structurally reminiscent of procaspase-8, has been established as a principal modulator of death-ligand-elicited apoptosis. It accomplishes this regulatory role by associating with FADD and/or caspase-8 or -10, in a ligand-dependent manner, thereby impeding cell death triggered by tumor necrosis factor-alpha (TNF-alpha), Fas-L, and TRAIL. This blockade prevents the formation of the death-inducing signaling complex (DISC) and, consequently, arrests the downstream propagation of the apoptotic enzymatic cascade [37]. Dapagliflozin, as indicated by recent investigations, induces apoptosis by downregulating cFLIP-L and destabilizing cFLIP-S, and may represent a promising therapeutic candidate for the management of human renal carcinoma [38].

Building upon this premise, we performed docking of caffeine into the c-FLIP binding cavity. Although the computed binding affinity of dapagliflozin was determined to be comparatively weaker (−6.5) than that of caffeine, the contacts established by dapagliflozin were limited to Van der Waals forces and pi–alkyl associations, whereas those formed by caffeine featured hydrogen bonds in addition to Van der Waals-type interactions and exhibited a closer resemblance to the contacts made by Procaspase-8. Accordingly, caffeine is predicted to function as an effective suppressor of cFLIP, a prediction confirmed by relative transcript quantification.

The enlargement of organ masses observed during the whole-animal experimental phase was conceivably driven by benzene-derived metabolites, which directly target these visceral organs and provoke free radical generation linked to hypertrophic tissue remodeling [39]. Nevertheless, the prompt normalization of organ weights achieved by all treatment modalities furnishes compelling evidence of the protective capacity of the nanomedicine against benzene-induced hypertrophy.

Benzene triggers acute myeloid leukemia through its metabolic byproducts, which include phenol, catechol, and hydroquinone. Cytomorphological examination reveals that benzene, acting via these cytotoxic intermediates, induces erythrocytosis, culminating in a diminished overall erythrocyte count alongside additional abnormalities such as eosinophilia and leukocytosis [40]. In a similar vein, owing to the array of mutations benzene inflicts on bone marrow progenitor cells that disrupt leukocyte maturation, the total leukocyte count escalates, leading to elevated numbers of circulating immature blast forms in the peripheral blood of leukemic subjects [41]. Parallel observations were documented in our own study as well. The delivery of diverse pharmacological protocols reinstated a physiological blood profile in the leukemic rodents, significantly attenuating erythrocytosis, eosinophilia, and leukocytosis [40]. Caffeine is documented to enforce G2/M phase arrest and programmed cell death in leukemic cell populations [42]. The decline in thrombocyte numbers detected in our investigation is most plausibly ascribed to the injurious consequences on bone marrow cellular constituents instigated by benzene inoculation. Of particular note, intervention with the nanomedicine substantially elevated platelet counts by mitigating thrombocytopenia [43].

Benzene also disrupts the physiological concentrations of ALP, ALT, and AST by generating ROS via its downstream metabolites, consistent with the liver being a principal target of benzene-mediated toxicity [42]. The decline in ALP activity observed in rats with benzene-induced leukemia can be attributed to the absence of

detectable leukocyte alkaline phosphatase (LAP) messenger RNA in AML. Meanwhile, the surge in ALT levels was most likely driven by aberrant hepatocyte expansion, which increases alanine transaminase enzyme output in the leukemic animals [44]. Similarly, circulating AST concentrations increased, serving as a biomarker of benzene-induced hepatocytotoxicity and hepatic parenchymal injury. Benzene dosing also pushed serum creatinine values above normal thresholds, foreshadowing acute renal compromise in the leukemic subjects [45]. Against this backdrop, our nano-formulation substantially normalized these deranged hepatic enzyme activities and creatinine benchmarks, an outcome plausibly rooted in diminished cytotoxic burden and heightened radical-scavenging capacity.

Gene expression profiling was carried out on homogenized hepatic tissue, given the liver's role as the central metabolic processing station for virtually all xenobiotic compounds, including benzene. STMN1, recognized as one of the transcripts most dramatically upregulated in AML, exhibited heightened expression in the benzene-challenged leukemic rats, providing genetic-level verification of leukemogenesis [46]. Intervention with CcNP attenuated benzene's impact by reducing STMN1 transcript abundance, potentially altering actin cytoskeletal function and microtubule polymerization dynamics within cells [47].

Inactivation of p53, a widely recognized tumor suppressor, is a frequent genetic aberration in malignancies. Within AML, P53 expression becomes dysregulated as a consequence of mutational events and DNA injury mediated by reactive oxygen species. Our nanoparticulate therapeutic, however, reinstated the disrupted P53 levels in the leukemic rodents, putatively through its cell-death-promoting and antioxidant attributes. Additionally, the documented capacity of caffeine to impede lipid peroxidation triggered by reactive oxygen intermediates may have contributed to this recovery, as previously noted by Devasagayam *et al*. [26].

The marked upregulation of GAPDH in the benzene-exposed cohort was likely a manifestation of heightened glycolytic flux, a metabolic signature that likewise constitutes an established hallmark of cancer [1, 48]. Application of our nano-formulation, along with other therapeutic regimens, re-established baseline GAPDH expression by correcting cellular energy metabolism and restraining the unchecked proliferation of transformed cells [49].

mTOR, which operates as a pivotal integrator of both intra- and extracellular cues governing fundamental processes including cellular enlargement, proliferative drive, and survival signaling, was similarly elevated in the benzene-dosed experimental groups. This kinase also orchestrates leukemic cell expansion, tumor-associated neovascularization, and the transcriptional output of vascular endothelial growth factor [50]. The underlying mechanism involves mTOR's recognized ability to recruit microRNAs that transcriptionally silence pro-apoptotic genes, thereby facilitating leukemogenesis [51]—our nanotherapeutic sharply reduced mTOR levels, an effect likely attributable to its apoptosis-promoting properties.

Rel A and Rel B, components of the NF-kappa B signaling axis, underpin cellular persistence in AML, as reflected by their elevated messenger RNA transcript levels during leukemogenic progression [52]. Doxorubicin, which triggers apoptotic cell death by generating ROS, suppressed RelB transcript abundance [53]. In the case of Rel A, however, the DNA lesions inflicted by doxorubicin paradoxically activated the canonical NF-κB cascade. This phenomenon fosters doxorubicin tolerance in leukemic populations and may account for the persistently elevated Rel A expression (in contrast to Rel B) documented in the doxorubicin-receiving animals. Nonetheless, the suppression of both NF-kappa B pathway indicators, Rel A and Rel B, by our nano-formulation—whether deployed singly or in combination with chemotherapy—points to its growth-restraining and tumor-antagonizing efficacy in the leukemic rodent model. This outcome is likely rooted in the established anti-survival and inhibitory actions of caffeine against Rel A and Rel B. These effects are presumably amplified in the nano-encapsulated format, as the MSNP scaffold enhances the bioavailability, biostability, and circulatory persistence of surface-adhered caffeine, in line with earlier reports [54].

When evaluating the contribution of programmed cell death, the TRAIL signaling cascade has remained among the most extensively scrutinized pathways. The heightened transcriptional activity of the TRAIL ligand in benzene-intoxicated rats is not unexpected, given that numerous benzene-derived compounds are recognized participants in TRAIL-mediated cell killing [55]. The overabundance of cFLIP dampens TRAIL-directed signaling in such leukemic animals [56]. The notably boosted expression of the TRAIL ligand, paired with reduced cFLIP levels, positions our nano-formulation as a robust modulator of the TRAIL pathway and a potent driver of apoptotic induction. This conclusion is further strengthened by the elevated DR5 expression observed in the nano-treated cohort. The co-administration of the nanomedicine with conventional chemotherapy resulted in even greater amplification of DR5 transcript levels, suggesting an interplay between the two [57]. A therapy-induced

increase in DR5 represents a constructive step toward TRAIL-orchestrated apoptosis via the extrinsic pathway. Nonetheless, upregulating death receptors in isolation is insufficient to trigger cell death; their functional organization into trimeric assemblies is equally essential for the execution of apoptotic signaling. Given that we detected no upregulation of either initiator or executioner caspases, we propose incorporating an agonistic antibody in future investigations to potentiate the functional competence of death receptors in eliciting apoptosis [58]. The heightened cytochrome c concentrations measured in the leukemic rats are indicative of accelerated mitochondrial release, a consequence of outer membrane compromise and ensuing cellular demise. Intervention with the assorted pharmacological protocols returned these levels to the physiological range, likely owing to antioxidant and broader cytoprotective mechanisms.

Conclusion

The integrated findings from both cell-free and animal-based experiments corroborate the nano-formulation's singular anti-leukemic capacity. This picture aligns closely with computational modeling outcomes that cast our nanomedicine as a powerful driver of TRAIL-DR5 protein assembly (pdb:1du3) and a blocker of the NF-kB p52/RelB/DNA transcriptional machinery. That said, additional investigative work remains necessary to validate the targeting fidelity, molecular discrimination, and physiological compatibility of this nanocarrier system, and to subject it to the rigors of clinical evaluation. Although an array of chemotherapeutic options aimed at acute myeloid leukemia is currently available on the market, their burdensome adverse effect profiles render them less than ideal choices for patient care. Our study presents a potential means of overcoming these drawbacks, as the therapeutic punch of caffeine against acute myeloid leukemia has been appreciably enhanced when delivered as a nano-architected medicine. This outcome further highlights the role that nanoparticulate platforms can play as exceptional enhancers, boosting the tumoricidal performance of naturally derived molecules while simultaneously mitigating the noxious collateral damage inflicted by standard chemotherapy.

Acknowledgments: We are thankful to the research supporting project number (RSPD2024R740), King Saud University, Riyadh, Saudi Arabia.

Conflict of Interest: None

Financial Support: Research supporting project number (RSPD2024R740), King Saud University, Riyadh, Saudi Arabia.

Ethics Statement: The Institutional Review Board of Quaid-i-Azam University ethically approved the study through Approval Letter No. #BEC-FBS-QAU2020-221, dated 10-01-2020.

References

1. Hanahan D, Weinberg RA. Hallmarks of cancer: The next generation. Cell. 2011;144:646-74.
2. Sahu B, Laakso M, Ovaska K, Mirtti T, Lundin J, Rannikko A, et al. Dual role of FoxA1 in androgen receptor binding to chromatin, androgen signalling and prostate cancer. EMBO J. 2011;30:3962-76.
3. Bennett JM, Catovsky D, Daniel MT, Flandrin G, Galton DA, Gralnick HR, et al. Proposals for the classification of the acute leukaemias French-American-British (FAB) co-operative group. Br J Haematol. 1976;33:451-8.
4. Paul AT, Jindal A. Nano-natural products as anticancer agents. In: Akhtar MS, Swamy MK, editors. Anticancer plants: Clinical trials and nanotechnology. Singapore: Springer; 2017. p. 27-50.
5. Tacar O, Sriamornsak P, Dass CR. Doxorubicin: An update on anticancer molecular action, toxicity and novel drug delivery systems. J Pharm Pharmacol. 2013;65:157-70.
6. Partridge AH, Burstein HJ, Winer EP. Side effects of chemotherapy and combined chemohormonal therapy in women with early-stage breast cancer. JNCI Monogr. 2001;2001:135-42.
7. Heckman MA, Weil J, De Mejia EG. Caffeine (1,3,7-trimethylxanthine) in foods: A comprehensive review on consumption, functionality, safety, and regulatory matters. J Food Sci. 2010;75:R77-87.
8. Calvo I, Gabrielli N, Iglesias-Baena I, Garcia-Santamarina S, Hoe KL. Genome-wide screen of genes required for caffeine tolerance in fission yeast. PLoS One. 2009;4:e6619.

9. Monteiro J, Alves MG, Oliveira PF, Silva BM. Pharmacological potential of methylxanthines: Retrospective analysis and future expectations. Crit Rev Food Sci Nutr. 2019;59:2597-625.
10. Sinha R, Kim GJ, Nie S, Shin DM. Nanotechnology in cancer therapeutics: Bioconjugated nanoparticles for drug delivery. Mol Cancer Ther. 2006;5:1909-17.
11. Slowing II, Trewyn BG, Giri S, Lin VY. Mesoporous silica nanoparticles for drug delivery and biosensing applications. Adv Funct Mater. 2007;17:1225-36.
12. Wu SH, Mou CY, Lin HP. Synthesis of mesoporous silica nanoparticles. Chem Soc Rev. 2013;42:3862-75.
13. Basak M, Rahman ML, Ahmed MF, Biswas B, Sharmin N. The use of X-ray diffraction peak profile analysis to determine the structural parameters of cobalt ferrite nanoparticles using Debye-Scherrer, Williamson-Hall, Halder-Wagner and Size-strain plot: Different precipitating agent approach. J Alloys Compd. 2022;895:162694.
14. Wang J, Wang H, Zhu R, Liu Q, Fei J, Wang S. Anti-inflammatory activity of curcumin-loaded solid lipid nanoparticles in IL-1β transgenic mice subjected to the lipopolysaccharide-induced sepsis. Biomaterials. 2015;53:475-83.
15. Nakamura K, Yamashita K, Itoh Y, Yoshino K, Nozawa S, Kasukawa H. Comparative studies of polyethylene glycol-modified liposomes prepared using different PEG-modification methods. Biochim Biophys Acta Biomembr. 2012;1818:2801-7.
16. Vojoudi H, Badiei A, Amiri A, Banaei A, Ziarani GM, Schenk-Joß K. Efficient device for the benign removal of organic pollutants from aqueous solutions using modified mesoporous magnetite nanostructures. J Phys Chem Solids. 2018;113:210-9.
17. Kondapuram S, Sarvagalla S, Coumar MS. Docking-based virtual screening using PyRx tool: Autophagy target Vps34 as a case study. In: Molecular docking for computer-aided drug design. Cambridge (MA): Academic Press; 2021. p. 463-77.
18. Trott O, Olson AJ. AutoDock Vina: Improving the speed and accuracy of docking with a new scoring function, efficient optimization, and multithreading. J Comput Chem. 2010;31:455-61.
19. Mirzaei H, Zarbafian S, Villar E, Mottarella S, Beglov D, Vajda S, et al. Energy minimization on manifolds for docking flexible molecules. J Chem Theory Comput. 2015;11:1063-76.
20. Dassault Systèmes BIOVIA. Discovery Studio Modelling Environment, Release 4.5. Los Angeles (CA): Scientific Research Publishing; 2015. p. 98-104.
21. Rath S, Sahu MC, Dubey D, Debata NK, Padhy RN. Which value should be used as the lethal concentration 50 (LC50) with bacteria? Interdiscip Sci Comput Life Sci. 2011;3:138-43.
22. Phatak RS, Pratinidhi AK, Hendre AS. Screening of some Indian household spices for comparative studies of antioxidant and antiradical activities by using in vitro models. Asian J Pharm Clin Res. 2015;8:431-8.
23. Moein S, Moein M, Khoshnoud MJ, Kalanteri T. In vitro antioxidant properties evaluation of 10 Iranian medicinal plants by different methods. Iran Red Crescent Med J. 2012;14:771.
24. Yamamoto T, Nozaki-Taguchi N, Chiba T. Analgesic effect of intrathecally administered orexin-A in the rat formalin test and in the rat hot plate test. Br J Pharmacol. 2002;137:170-6.
25. Samuelson BT, Cuker A, Siegal DM, Crowther M, Garcia DA. Laboratory assessment of the anticoagulant activity of direct oral anticoagulants: A systematic review. Chest. 2017;151:127-38.
26. Xu J, Zhou P, Wang W, Sun A, Guo F. RelB, together with RelA, sustains cell survival and confers proteasome inhibitor sensitivity of chronic lymphocytic leukemia cells from bone marrow. Int J Mol Med. 2014;34:77-92.
27. Institute of Laboratory Animal Resources, Committee on Care and Use of Laboratory Animals. Guide for the care and use of laboratory animals. Washington (DC): US Department of Health and Human Services, Public Health Service, National Institutes of Health; 1986.
28. Sathpathi S, Mohanty AK, Satpathi P, Mishra SK, Behera PK, Patel G, et al. Comparing Leishman and Giemsa staining for the assessment of peripheral blood smear preparations in a malaria-endemic region in India. Malar J. 2014;13:512. doi:10.1186/1475-2875-13-512
29. Chomczynski P. Reagents and methods for isolation of purified RNA. US Patent 7794932. 2010 Sep 14.
30. Stellwagen NC. DNA gel electrophoresis. In: Nucleic acid electrophoresis. Berlin: Springer; 1998. p. 1-53.
31. Zhang Y, Zhi Z, Jiang T, Zhang J, Wang Z, Wang S. Spherical mesoporous silica nanoparticles for loading and release of the poorly water-soluble drug telmisartan. J Control Release. 2010;145:257-63.

32. Ferreira G, Hernandez-Martinez AR, Pool H, Molina G, Cruz-Soto M, Luna-Barcenas G, et al. Synthesis and functionalization of silica-based nanoparticles with fluorescent biocompounds extracted from Eysenhardtia polystachya for biological applications. Mater Sci Eng C Mater Biol Appl. 2015;57:49-57.
33. Jiao Y, Guo J, Shen S, Chang B, Zhang Y, Jiang X, et al. Synthesis of discrete and dispersible hollow mesoporous silica nanoparticles with tailored shell thickness for controlled drug release. J Mater Chem. 2012;22:17636-43.
34. Nandiyanto ABD, Kim SG, Iskandar F, Okuyama K. Synthesis of spherical mesoporous silica nanoparticles with nanometer-size controllable pores and outer diameters. Microporous Mesoporous Mater. 2009;120:447-53.
35. Das S, Tripathi N, Preet R, Siddharth S, Nayak A, Bharatam PV, et al. Quinacrine induces apoptosis in cancer cells by forming a functional bridge between TRAIL-DR5 complex and modulating the mitochondrial intrinsic cascade. Oncotarget. 2017;8:248-67.
36. Fusco AJ, Huang DB, Miller D, Wang VY, Vu D, Ghosh G. NF-kappaB p52:RelB heterodimer recognizes two classes of kappaB sites with two distinct modes. EMBO Rep. 2009;10:152-9.
37. Safa AR, Day TW, Wu CH. Cellular FLICE-like inhibitory protein (C-FLIP): A novel target for cancer therapy. Curr Cancer Drug Targets. 2008;8:37-46.
38. Jang JH, Lee TJ, Sung EG, Song IH, Kim JY. Dapagliflozin induces apoptosis by downregulating cFLIPL and increasing cFLIPS instability in Caki-1 cells. Oncol Lett. 2022;24:401.
39. Rana S, Verma Y. Biochemical toxicity of benzene. J Environ Biol. 2005;26:157-68.
40. Hallenbeck WH, Cunningham-Burns KM. Carbamates. In: Pesticides and human health. New York: Springer; 1985. p. 30-32.
41. Greenwood MJ, Seftel MD, Richardson C, Barbaric D, Barnett MJ, Bruyere H, et al. Leukocyte count as a predictor of death during remission induction in acute myeloid leukemia. Leuk Lymphoma. 2006;47:1245-52.
42. Ito K, Nakazato T, Miyakawa Y, Yamato K, Ikeda Y, Kizaki M. Caffeine induces G2/M arrest and apoptosis via a novel p53-dependent pathway in NB4 promyelocytic leukemia cells. J Cell Physiol. 2003;196:276-83.
43. Olsson M, Bruhns P, Frazier WA, Ravetch JV, Oldenborg PA. Platelet homeostasis is regulated by platelet expression of CD47 under normal conditions and in passive immune thrombocytopenia. Blood. 2005;105:3577-82.
44. Farrow AC, Buchanan GR, Zwiener RJ, Bowman WP, Winick NJ. Serum aminotransferase elevation during and following treatment of childhood acute lymphoblastic leukemia. J Clin Oncol. 1997;15:1560-6.
45. Lahoti A, Kantarjian H, Salahudeen AK, Ravandi F, Cortes JE, Faderl S, et al. Predictors and outcome of acute kidney injury in patients with acute myelogenous leukemia or high-risk myelodysplastic syndrome. Cancer. 2010;116:4063-8.
46. Handschuh L, Kaźmierczak M, Milewski MC, Góralski M, Łuczak M, Wojtaszewska M, et al. Gene expression profiling of acute myeloid leukemia samples from adult patients with AML-M1 and AML-M2 through boutique microarrays, real-time PCR and droplet digital PCR. Int J Oncol. 2018;52:656-78.
47. Wu N, Gao N, Fan D, Wei J, Zhang J, An J. miR-223 inhibits dengue virus replication by negatively regulating the microtubule-destabilizing protein STMN1 in EAhy926 cells. Microbes Infect. 2014;16:911-22.
48. Devasagayam TP, Kamat JP, Mohan H, Kesavan PC. Caffeine as an antioxidant: Inhibition of lipid peroxidation induced by reactive oxygen species. Biochim Biophys Acta Biomembr. 1996;1282:63-70.
49. Ward PS, Thompson CB. Metabolic reprogramming: A cancer hallmark even Warburg did not anticipate. Cancer Cell. 2012;21:297-308.
50. Jiang GJ, Wang K, Miao DQ, Guo L, Hou Y, Schatten H, et al. Protein profile changes during porcine oocyte aging and effects of caffeine on protein expression patterns. PLoS One. 2011;6:e28996.
51. Fruchon S, Kheirallah S, Al Saati T, Ysebaert L, Laurent C, Leseux L, et al. Involvement of the Syk-mTOR pathway in follicular lymphoma cell invasion and angiogenesis. Leukemia. 2012;26:795-805.
52. Martelli AM, Evangelisti C, Chappell W, Abrams SL, Bäsecke J, Stivala F, et al. Targeting the translational apparatus to improve leukemia therapy: Roles of the PI3K/PTEN/Akt/mTOR pathway. Leukemia. 2011;25:1064-79.
53. Tapia MA, González-Navarrete I, Dalmases A, Bosch M, Rodriguez-Fanjul V, Rolfe M, et al. Inhibition of the canonical IKK/NFκB pathway sensitizes human cancer cells to doxorubicin. Cell Cycle. 2007;6:2284-92.

54. Szatkowska P, Koba M, Koslinski P, Szablewski M. Molecularly imprinted polymers' applications: A short review. Mini Rev Org Chem. 2013;10:400-8.
55. Ahn Y, Lee S, Park CS, Jang HJ, Lee JH, Park BG, et al. Diethylamino-curcumin mimic with trizolyl benzene enhances TRAIL-mediated cell death on human glioblastoma cells. Mol Cell Toxicol. 2018;14:241-5.
56. Sayers TJ, Brooks AD, Koh CY, Ma W, Seki N, Raziuddin A, et al. The proteasome inhibitor PS-341 sensitizes neoplastic cells to TRAIL-mediated apoptosis by reducing levels of c-FLIP. Blood. 2003;102:303-10.
57. Mérino D, Lalaoui N, Morizot A, Schneider P, Solary E, Micheau O. Differential inhibition of TRAIL-mediated DR5-DISC formation by decoy receptors 1 and 2. Mol Cell Biol. 2006;26:7046-55.
58. El-Gazzar A, Perco P, Eckelhart E, Anees M, Sexl V, Mayer B, et al. Natural immunity enhances the activity of a DR5 agonistic antibody and carboplatin in the treatment of ovarian cancer. Mol Cancer Ther. 2010;9:1007-18.